Optical Read-Out of the Electrical Switching of Cobalt-Terpyridine-BODIPY Molecules Immobilized as Single Layer on ITO

Kévin Magra, Jean-frédéric Audibert, Diana Dragoe, Talal Mallah, Fabien Miomandre, Marie-laure Boillot

ADVANCED OPTICAL MATERIALS
www.advopticalmat.de

Optical Read-Out of the Electrical Switching of Cobalt-Terpyridine-BODIPY Molecules Immobilized as Single Layer on ITO

Kévin Magra, Jean-Frédéric Audibert, Diana Dragoe, Talal Mallah, Fabien Miomandre,* and Marie-Laure Boillot**

A single layer of a dyad made of a cobalt(II) bis-terpyridine complex functionalized with a Boron-dipyrromethene (BODIPY) fluorophore on transparent Indium Tin Oxide (ITO) electrode is prepared. A modulation of the photoluminescence intensity of the fluorophore upon the application of an electric stimulus on the ITO electrode that supports 10 picomoles of molecules is demonstrated. The intensity of the fluorescence intensity decreases when the cobalt is at the oxidation state +III, due to Co^{III} oxidative quenching of BODIPY emission that has a higher driving force than the Co^{II} reductive quenching initially responsible for the low fluorescence intensity of the chemisorbed dyad.

1. Introduction

Molecular dyads based on electrochemically active and luminescent components with tunable optical response of one moiety resulting from the charge state change of the other part are among the most studied molecular switches.[1,2] Such molecular switch was first reported in 1993,[3] and a diversity of such molecules were eventually designed.[4–6] Among them, metal complexes played an important role, either as the redox switch or the luminophore,[5,7] to generate electrofluorochromic systems in which the luminescence properties can be electrochemically controlled and tuned. In such dyads, when the metal complex is electroactive, an electrical stimulus not only changes the charge of the metal ion but may also promote spin-crossover type conversion (high spin to low spin and vice versa),[8] providing electronic states with relatively large energy barriers, and hence molecular bistability. To the best of our knowledge, the investigations of such functional molecules that can be electrochemically stimulated and optically detected were performed only in solution and not at the single molecule level or as monolayers. In this context, the design of Co complexes that present tunable redox and spin-state switching properties as well as processability, was considered. One decisive advantage is the possibility to control the magnetic behavior from an electrical input with an optical output. Ultrathin films of covalently immobilized Co complexes on conductive substrates were investigated for a variety of purposes: catalysis,[9,10] electron conduction,[11] molecular transistor,[12] photoelectric conversion,[13,14] electrochromism,[15,16] switchable materials.[17–19]

One of the bottlenecks is to reduce the delay time between applying the electrical stimulus and reading the optical response that must be intense enough. Electrochemical scanning tunneling microscopy methods,[20] or the Electrochemistry/Atomic force microscopy coupling were developed for locally probing processes at the molecular scale, but general applications are limited by the slow time scales inherent to such techniques. The coupling between electrochemistry and fluorescence microscopy allows monitoring in a non-invasive, synchronous and very sensitive way, the electrochemical and the fluorescence signals arising ultimately from single molecules located at the proximity of the electrode.[21,22] It is worth noting that the electrofluochromism of a single layer,[23] and of isolated non-dyad molecules,[24] have been recently reported, demonstrating the feasibility of such sensitive detection.

We report here, the detection at the single layer level of the reversible electrical switching of original heteroleptic cobalt(II) complexes functionalized with a sensitive BODIPY fluorophore,[25] covalently immobilized on an Indium Tin Oxide (ITO) electrode (see in **Figure 1**a). We use well-established terpyridine and fluorescent BODIPY building blocks to design

K. Magra, D. Dragoe, T. Mallah, M.-L. Boillot
Institut de Chimie Moléculaire et des Matériaux d'Orsay
CNRS
Université Paris-Saclay
UMR 8182, Orsay 91400, France
E-mail: talal.mallah@universite-paris-saclay.fr;
marie-laure.boillot@universite-paris-saclay.fr
J.-F. Audibert, F. Miomandre
École Normale Supérieure Paris-Saclay
CNRS
PPSM
Université Paris-Saclay
Gif-sur-Yvette 91190, France
E-mail: mioman@ens-cachan.fr

The ORCID identification number(s) for the author(s) of this article can be found under https://doi.org/10.1002/adom.202301128

DOI: 10.1002/adom.202301128

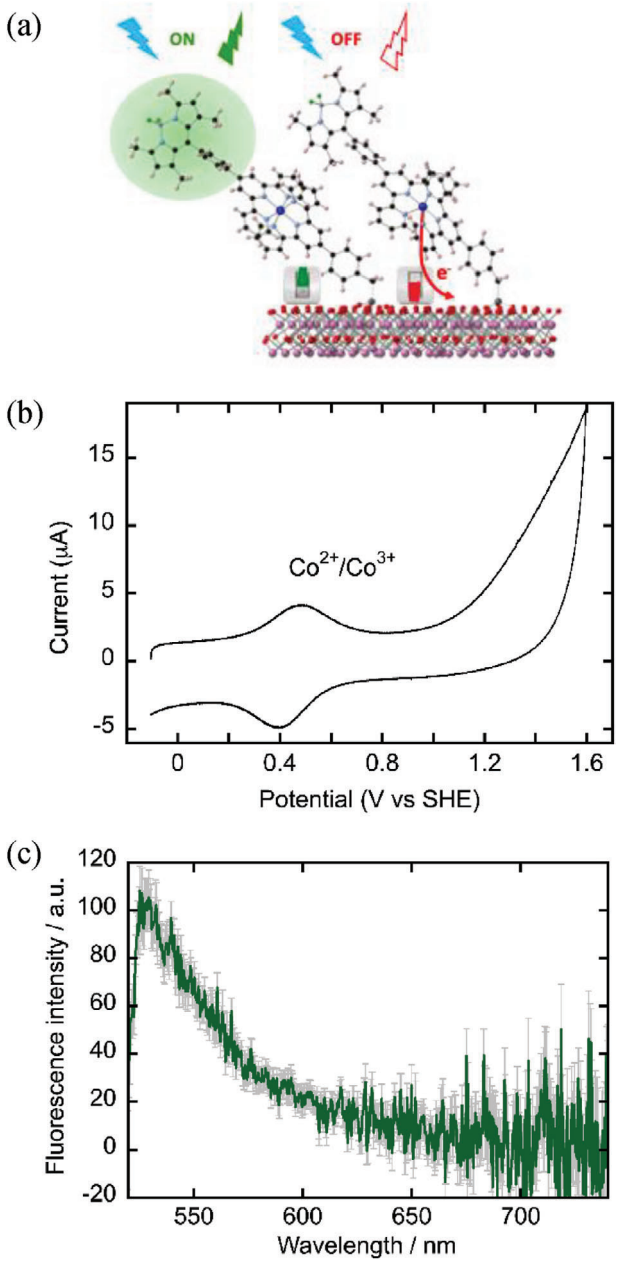

Figure 1. a) Illustration of the concept based on functional monolayers of $[(L_a)Co^{II}(L_c)](BF_4)_2$ covalently immobilized on the ITO electrode; b) Cyclic voltammogram of the monolayer ITO-$[(L_a)Co^{II}$(tpy-Ph-BODIPY)] (in $CH_3CN/Bu_4N^+PF_6^-$ (0.1 M), 25 °C); c) Corrected fluorescence emission spectra (——, green) and its corresponding amplitude standard deviation (——, grey) at the monolayer-electrolyte interface averaged within 2 sec after the start of the laser irradiation at 474 nm.

the new dissymmetric electrofluorochromic dyad.[13,26] The characterization and the study of the functionalized surfaces are achieved with cyclic voltammetry (CV) and emission spectrophotometry measurements using a set-up consisting in a fluorescence microscope coupled to an electrochemical cell. With this set-up, fluorescence spectra under electrochemical control can be recorded to investigate the possibility to electrically switch the magnetic properties of the complex with an optical readout of its redox state.

2. Results and Discussion

2.1. Functional Molecule and ITO-Anchored Monolayer

The functional molecules were assembled on ITO using a phosphonate anchoring group following a reported sequential approach (**Schemes 1** and S1, S2, S3, and Figure S1 (Supporting Information), for ligands synthesis and single layer preparation).[13,26,27]

We use X-ray Photoelectron Spectroscopy (XPS) to analyze the monolayer (Figure S2, Supporting Information). The survey spectrum (three different regions) confirms the presence of Co, C, N, and P elements along with In, Sn and O signals of ITO. The core-level spectrum of Co2p consists of two main peaks (spin-orbit coupling components): $Co2p_{3/2}$ at 781.4 ± 0.2 eV and $Co2p_{1/2}$ at 796.4 ± 0.2 eV and their corresponding satellite peaks. The $Co2p_{3/2}$ peak, separated by ≈6 eV from its satellite indicates the presence of Co^{II} state.[28] The N1s peak at 399.8 ± 0.2 eV is typical for imine type nitrogen atoms.[29] The N/Co atomic ratio determined from the area of the $Co2p_{3/2}$ and the N1s bands varies (three different spots) from 7.4 to 8.3 consistently with the theoretical value of 8. The $P2p_{3/2}$ component of the P2p core-level doublet is at 133 ± 0.2 eV, corresponding to phosphate type bond.[30] These data demonstrate the success of the stepwise grafting process of the dyad on ITO. The homoleptic complex $[Co^{II}$(tpy-Ph-BODIPY)$_2](PF_6)_2$ was also prepared and its electrochemical and optical behavior was used as a reference (Scheme S4; Figures S1, S3 and S4, Supporting Information). The CV of this complex recorded in CH_3CN (Figure S3, Supporting Information) shows the redox processes centered on the metal ion (reversible $Co^{+3/+2}$ couple at $E_{1/2}$ = 0.52 V/SHE, non-reversible $Co^{+2/+1}$ couple at E_{pc} = −0.43 V/SHE) and those associated to the BODIPY moiety ($BODIPY^{+1/0}$ couple at E_{pa} = 1.47 V/SHE, reversible $BODIPY^{0/-1}$ couple at $E_{1/2}$ = −0.79 V/SHE).[26,31,32] The UV–vis absorption spectrum (Figure S4, Supporting Information) is dominated by the intense intra-ligand transition of BODIPY at 499 nm while the absorption of the ttpy and $[Co(ttpy)_2]^{2+}$ chromophores (ttpy = 4′-phenyl-2,2′:6,2′′-terpyridine) is observed at higher energies. The emission spectrum consists in the BODIPY fluorescence at 515 nm that intersects the absorption peak at $E_{0\text{-}0}$ = 2.45 eV.[26]

2.2. Electrochemistry and Fluorescence of Monolayer

The electrochemical behavior of the monolayer on ITO-$[(L_a)Co^{II}(L_c)](BF_4)_2$ was probed by CV (Figure 1b; Figure S3a, Supporting Information). The reversible signature of the Co^{II}/Co^{III} couple ($E_{1/2} = (E_{pa}+E_{pc})/2$ = 0.44 V/SHE) has a symmetrical bell-shape that characterizes the behavior of immobilized redox species. It is consistent with the oxidation potential of Co ([0.44-0.56] V/SHE) for related monolayer architectures.[13,14,33,34] The peak-to-peak separation (ΔE_{pp} = 90 mV) indicates a marked slowing down of the electron transfer. ΔE_{pp} tends to grow with the reorganization (counter ion, solvation) upon the redox process of immobilized systems.[35] The broadening may result from

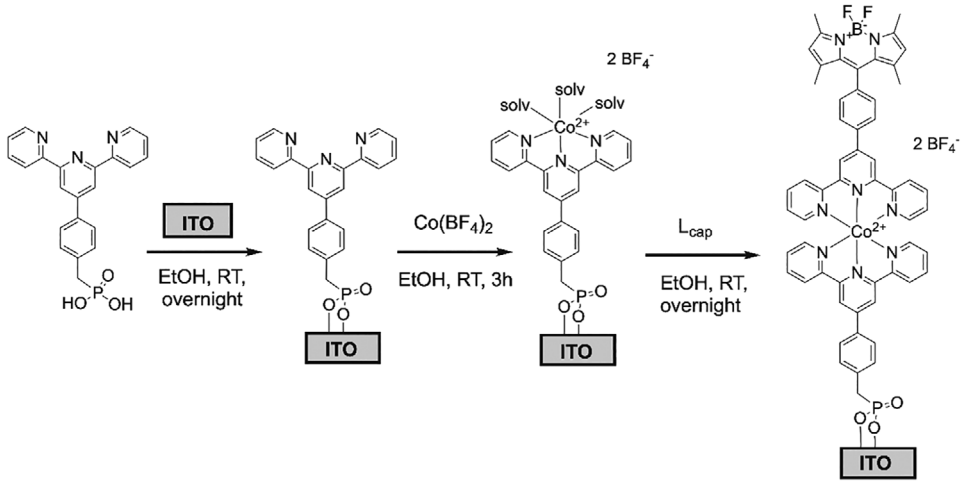

Scheme 1. Synthetic method followed for the anchoring of the functional complex $[(L_a)Co^{II}(L_c)](BF_4)_2$ on ITO (L_c = BODIPY-Ph-tpy and $L_a = O_3P\text{-}CH_2\text{-}$Ph-tpy).

large inner reorganization energy (in the Marcus sense) or an electrochemical square scheme involving a slow electron self-exchange,[36] between Co^{II} and Co^{III} at the electrode surface.[8] Interestingly, the Co peak is well separated from the one associated to the irreversible oxidation of the BODIPY moiety (>1.51 V/SHE). The linear variation of the anodic peak current of Co with the potential scan rate (Figure S3b and S3c, Supporting Information) confirms a redox process which is not diffusion-limited but controlled by the number of immobilized redox species and yields to a surface concentration Γ of 0.05-0.08 × 10^{-10} moles cm^{-2} (≈10 picomoles cm^{-2}). This value corresponds to a monolayer with 4%–6% saturated coordination sites relatively to the estimated saturation coverage of the electrode, $\Gamma_{sat} = 1.37 \times 10^{-10}$ moles cm^{-2}, close to those reported (0.06-0.7 × 10^{-10} moles cm^{-2}).[13,33,34]

2.3. Photoluminescence and Electrofluorochromism of the Monolayer

We probed the photoluminescence (PL) and electrofluorochromism (EFC) of the monolayer with an excitation at 474 nm and an electrochemical modulation between two values of the potential corresponding to the Co redox switch, but remaining below the oxidation potential of BODIPY. A fluorescence signal was observed in the 520–670 nm range for the modified ITO in contact with air (Figure S4, Supporting Information) assigned to a weak BODIPY emission that was absent for bare ITO. It was also recorded when the modified ITO electrode is in contact with an electrolyte solution (Figure 1c). One issue that must be considered when applying the potential signal supposed to monitor the fluorescence intensity is the gradual bleaching of this signal upon continuous irradiation that is especially strong with a monolayer.

To test the homogeneity of the monolayer, bleaching kinetic curves were recorded at various positions for the same sample (Figure S4 and Table S1, Supporting Information). For the 5 recorded positions, the maximal value for the integrated intensity in the emission range can be averaged to I_{max} = 15 212 ± 543, indicating a good homogeneity of the sample. The bleaching kinetics were fitted with a three exponentials function and an apparent rate constant of 0.01 s^{-1}. A similar analysis was conducted for the monolayer in contact with the electrolyte (Figure S5, Supporting Information), with a final rate constant of 0.04 s^{-1}, showing a more efficient bleaching in the presence of the electrolyte, as expected especially if photoinduced charged processes are involved.

The electrofluorochromic properties of the monolayer were investigated by applying successive potential steps between −0.03 and +0.87 V/SHE (Co^{II}/Co^{III} redox window) for 3 successive cycles back and forth, under illumination (Figures S6 and S7, Supporting Information). The green curve (**Figure 2**) represents the extracted contribution of the electrochemical modulation to the variation of the fluorescence intensity after normalization by the bleaching component. To do so, the raw fluorescence variations

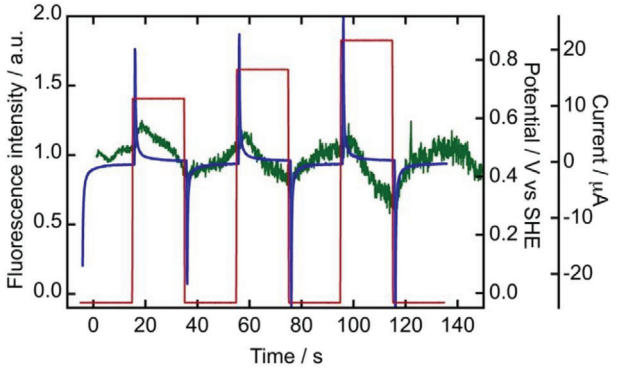

Figure 2. Intensity profile corrected (normalized) from bleaching profile. Simultaneous variation of fluorescence intensity (——, green) and current (——, blue) for a monolayer ITO-$[(L_a)Co^{II}$(tpy-Ph-BODIPY)] in contact with an electrolyte when the potential values (——, red) vary in a staircase manner between −0.03 and +0.87 V /SHE (6 cycles of 20 s). The fluorescence intensity versus time plots were corrected as described in Figure S6 from the decay resulting from the sole photobleaching of Co^{II}.

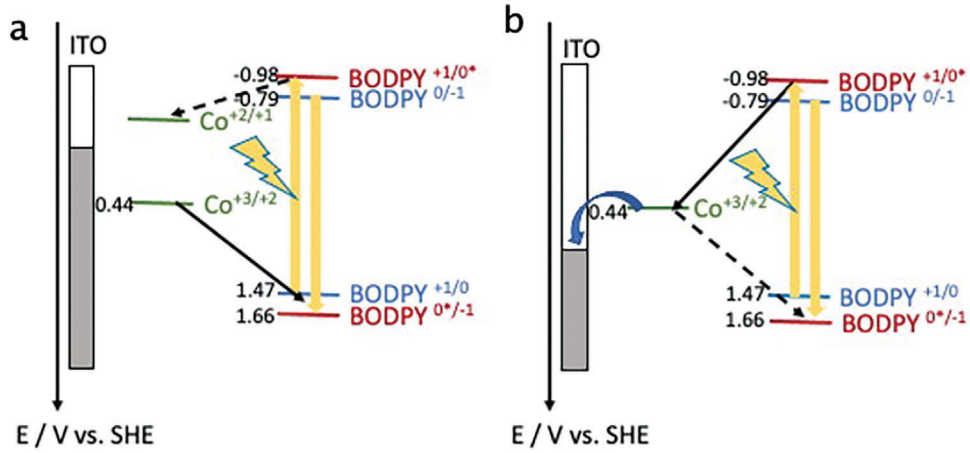

Figure 3. Diagram of the photoinduced electron transfer processes taking place at the modified electrode in contact with the electrolyte upon the photoexcitation at 470 nm, a) in the absence of polarization (open circuit) and b) when the electrode is polarized at potentials higher than $E°(Co^{III}/Co^{II})$. The values of $E°(BODIPY^{+1/0*}$-Ph-tpy) and $E°(BODIPY^{0*/-1}$-Ph-tpy) are based on the calculation with the Rehm and Weller equation and $E_{0\text{-}0} = 2.45$ eV (Tables S2 and S3, Supporting Information).

are recorded and fitted by the same three exponentials function as previously in the absence of electrochemical signal. This fit is applied to the data in the mask regions corresponding to the initial drop before starting the switch and to the plateau values at the end of each cycle (Figure S6, Supporting Information). The apparent rate constant extracted from the fit is the same as in absence of electrochemical signal (0.04 s^{-1}). The modulation of the emission intensity due to the electrochemical modulation corresponds, therefore, to the difference between the raw intensity values and those from the bleaching kinetic fit and results in the green curve. The first cycle presents singularities (not shown here), like a spontaneous increase in fluorescence regardless of the direction of the potential switching, and a plateau of fluorescence intensity for the Co^{II} form, suggesting a run-in stage due to structural or/and electronic factors that evolve with the formation of a new equilibrium state. In the following cycles, however, the trend is clearly an emission drop when oxidizing Co^{II} to Co^{III} followed by fluorescence recovery upon back reduction of Co^{III} to Co^{II} Moreover, the amplitude of the intensity modulation for each cycle follows the applied potential, becoming larger when the potential is more positive, in relation with a higher value of the Co^{III}/Co^{II} ratio compared to previously. This is a good indication that the green curve is actually an exact representation of the electrochemical modulation of the emission intensity.

This fluorescence intensity drop upon oxidation corresponds to a more efficient quenching of the BODIPY emission by the diamagnetic Co^{III} than by the paramagnetic Co^{II}. This behavior reported in valence-tautomeric analogues,[37,38] is a consequence of competitive processes (energy transfer and / or electron transfer) that may occur in the two forms. To analyze the role of the different sub-units in the photoinduced electron transfer (PET) mechanisms,[39,40] we considered the redox properties of ITO-[$(L_a)Co^{II}$(tpy-Ph-BODIPY)] (Figure 1; Figures S3a and S8, Supporting Information), those of the homoleptic analogue $[Co(L_c)_2](PF_6)_2$ (Figure S3d) and the estimates of the excited state redox potentials based on the Rehm and Weller equations. Different intramolecular reactions were found to be associated to negative free enthalpy values (**Figure 3**, Tables S2 and S3, Supporting Information). The intramolecular electron transfer between BODIPY* and the Co^{II} ion (Equation 1) is thermodynamically favored ($\Delta G \approx -1.14/-1.22^{ITO}$ eV) but a faster PET takes place between BODIPY* and the Co^{III} ion (Equation 2) ($\Delta G \approx -1.50/-1.42^{ITO}$ /eV) which dominates the kinetics of the process. The data extracted from the study of $[Co^{II}(L_c)_2](PF_6)_2$ in solution also suggest a competitive pathway depending on the kinetics of the electron transfer toward the electrode and that of the intramolecular transfer between BODIPY* and Co^{II} (Equation 3). This process (Equation 3) that leads to potentially non-stable Co^{I} intermediates is much less energetically favored ($\Delta G \approx -0.55$ eV). The competing mechanism involving energy transfer can be reasonably excluded because no significant variation of absorption at the excitation wavelength or in the emission range has been observed for the homoleptic complex when the applied potential lies in the range of cobalt oxidation only (Figure S9, Supporting Information). We can reasonably assume that the large driving force ($\Delta G > 1.4$ eV) for the electron transfer between $BODIPY^{0*/-1}$ and Co^{III}/Co^{II} makes this process dominant over other pathways.[41] The final outcome (Figure 3) thus consists in a reductive quenching of BODIPY* by Co^{II} in the absence of electrochemical signal (ON state), becoming replaced by a more efficient oxidative quenching of BODIPY* by Co^{III} when the electrode is polarized at potentials higher than 0.6 V/SHE (OFF state). Similar results for dyads involving a ruthenium redox center likely to quench the emission of porphyrins were already reported in solution, confirming the effectiveness of such mechanism.[25,42,43]

$$\mathrm{ITO} - \left[\left(L_a\right) Co^{II}\left(\mathrm{tpy-Ph-BODIPY}*\right)\right] \rightarrow \mathrm{ITO} - \left[\left(L_a\right) Co^{III}\left(\mathrm{tpy-Ph-BODIPY}^{\bullet -}\right)\right] \quad (1)$$

$$\mathrm{ITO} - \left[\left(L_a\right) Co^{III}\left(\mathrm{tpy-Ph-BODIPY}^{\bullet -}\right)\right] \rightarrow \mathrm{ITO} - \left[\left(L_a\right) Co^{II}\left(\mathrm{tpy-Ph-BODIPY}\right)\right] \quad (1')$$

$$\mathrm{ITO} - \left[\left(\mathrm{L_a}\right)\mathrm{Co^{III}}\left(\mathrm{tpy-Ph-BODIPY^{*}}\right)\right] \rightarrow \mathrm{ITO} - \left[\left(\mathrm{L_a}\right)\mathrm{Co^{II}}\left(\mathrm{tpy-Ph-BODIPY^{\bullet+}}\right)\right] \quad (2)$$

$$\mathrm{ITO} - \left[\left(L_a\right)\mathrm{Co^{II}}\left(\mathrm{tpy-Ph-BODIPY^{\bullet+}}\right)\right] \rightarrow \mathrm{ITO} - \left[\left(\mathrm{L_a}\right)\mathrm{Co^{III}}\left(\mathrm{tpy-Ph-BODIPY}\right)\right] \quad (2')$$

$$\mathrm{ITO} - \left[\left(\mathrm{L_a}\right)\mathrm{Co^{II}}\left(\mathrm{tpy-Ph-BODIPY^{*}}\right)\right] \rightarrow \mathrm{ITO} - \left[\left(\mathrm{L_a}\right)\mathrm{Co^{I}}\left(\mathrm{tpy-Ph-BODIPY^{\bullet+}}\right)\right] \quad (3)$$

$$\mathrm{ITO} - \left[\left(\mathrm{L_a}\right)\mathrm{Co^{I}}\left(\mathrm{tpy-Ph-BODIPY^{\bullet+}}\right)\right] \rightarrow \mathrm{ITO} - \left[\left(\mathrm{L_a}\right)\mathrm{Co^{II}}\left(\mathrm{tpy-Ph-BODIPY}\right)\right] \quad (3')$$

3. Conclusion

The results reported in this paper made the proof of concept of the optical read-out of the charge state of Co-containing dyad complexes grafted on ITO as a single monolayer, with a concentration of ≈10 picomoles cm^{-2}. They also demonstrate that when the electrode is polarized to generate the Co^{III} species, the electron transfer with the excited state of BODIPY is thermodynamically favored leading to a more efficient quenching of its photoluminescence than for the Co^{II} species, which is at the origin of this optical readout. The modulation of the intensity of the fluorescence emission can be further enhanced by adequately functionalizing the terpyridine ligand to better stabilize the Co^{III} state. Also, the BODIPY fluorophore can be modified in order to reduce the bleaching process that makes the analysis of the data complex. We are currently working in this direction.

4. Experimental Section

Solvents and commercially available reactants were used as received. NMR spectroscopic data were recorded on a DRX360 Bruker spectrophotometer and referenced to the solvent or TMS signal. High Resolution Mass spectrometry data were collected with a Bruker micrOTOF-Q spectrophotometer using Electrospray as ion source.

Synthetic procedures and analytical data of Ligands L_a and L_c are given in the Supporting Information.[13,26] The homoleptic complex $[Co^{II}(L_c)_2](PF_6)_2$ was synthesized by refluxing in CH_3OH a mixture of L_c and $CoCl_2.6H_2O$ (2:1 molar ratio) during 4 h. The solid, precipitated by the addition of KPF_6 in water, was dried in vacuum at 80 °C. HRMS (ESI) *m/z*: calcd for $C_{68}H_{56}B_2CoF_4N_{10}-2PF_6$, 584.7066; found, 584.7047. The preparation of monolayers was carried out via successive steps of impregnation, rinsing and sonication, and then drying, which began first with the immobilization of L_a, then the coordination of Co ions and finally the saturation of the coordination sphere with the capping ligand L_c. All the details and XPS characterizations by X-ray photoelectron spectroscopy (XPS) are given in the Supporting Information.

The XPS measurements were performed on a K-Alpha spectrometer from ThermoFischer, equipped with a monochromated X-ray Source (Al Kα, 1486.68 eV). UV–vis spectra were recorded with an Agilent Cary 3000 spectrophotometer. Fluorescence Microscopy and Electrofluorochromic data were recorded at room temperature using a homemade three electrodes spectroelectrochemical cell (CE: Pt wire, RE: Ag/Ag/Cl wire; WE: ITO plate) on top of an inverted optical microscope Ti Eclipse (Nikon). CV measurements were carried out with a VersaSTAT 4 (Ametek) potentiostat driven by VersaStudio software (Ametek). Samples are illuminated in wide-field mode on the microscope with a pulsed laser diode at 474 nm. Fluorescence intensity is collected through a longpass emission filter (LP 520 nm) and the bleaching kinetics are recorded with an SD2000 spectrophotometer (Ocean Optics) at 9 ps.

Supporting Information

Supporting Information is available from the Wiley Online Library or from the author.

Acknowledgements

M.-L.B. and F.M. thank the CHARM3AT Labex for the financial support and the post-Doc grant (ANR-11-IDEX-0003-02, 2019-003068 Project). The French Ministry of Research, the Centre National de la Recherche Scientifique, and the Groupement de Recherche CNRS -Photo-Electro-Stimulation- are acknowledged.

Conflict of Interest

The authors declare no conflict of interest.

Data Availability Statement

The data that support the findings of this study are available from the corresponding author upon reasonable request.

Keywords

cobalt, dyads, electrochemistry, electrofluorochromism, fluorescence, monolayer

Received: May 15, 2023
Revised: September 28, 2023
Published online:

[1] J. Otsuki, T. Akasaka, K. Araki, *Coord. Chem. Rev.* **2008**, *252*, 32.
[2] K. Nakamura, K. Kanazawa, N. Kobayashi, *J. Photochem. Photobiol. C: Photochem. Rev.* **2022**, *50*, 100486.
[3] V. R. Goulle, A. Harriman, J.-M. Lehn, *J. Chem. Soc. Chem. Commun.* **1993**, 1034.
[4] H. Al-Kutubi, H. R. Zafarani, L. Rassaei, K. Mathwig, *Eur. Polym. J.* **2016**, *83*, 478.
[5] Y. Zhuang, S. Guo, Y. Deng, S. Liu, Q. Zhao, *Chemistry – An Asian J.* **2019**, *14*, 3791.
[6] P. Audebert, F. Miomandre, *Chem. Sci.* **2013**, *4*, 575.
[7] Y. Kim, K. Kubo, *Pure Appl. Chem.* **2023**, *95*, 707.
[8] J. W. Turner, F. A. Schultz, *Coord. Chem. Rev.* **2001**, *219*, 81.
[9] A. Krawicz, J. Yang, E. Anzenberg, J. Yano, I. D. Sharp, G. F. Moore, *J. Am. Chem. Soc.* **2013**, *135*, 11861.
[10] B. Ma, G. Chen, C. Fave, L. Chen, R. Kuriki, K. Maeda, O. Ishitani, T.-C. Lau, J. Bonin, M. Robert, *J. Am. Chem. Soc.* **2020**, *142*, 6188.
[11] H. Maeda, R. Sakamoto, H. Nishihara, *Coord. Chem. Rev.* **2017**, *346*, 139.

[12] J. Tang, Y. Wang, J. E. Klare, G. S. Tulevski, S. J. Wind, C. Nuckolls, *Angew. Chem., Int. Ed.* **2007**, *46*, 3892.
[13] R. Farran, L. Le Quang, D. Jouvenot, F. Loiseau, R. Pansu, A. Deronzier, J. Chauvin, *Inorg. Chim. Acta* **2017**, *454*, 197.
[14] L. Le-Quang, R. Farran, Y. Lattach, H. Bonnet, H. Jamet, L. Guérente, E. Maisonhaute, J. Chauvin, *Langmuir* **2018**, *34*, 5193.
[15] K. Takada, R. Sakamoto, S.-T. Yi, S. Katagiri, T. Kambe, H. Nishihara, *J. Am. Chem. Soc.* **2015**, *137*, 4681.
[16] N. O. Laschuk, R. Ahmad, I. I. Ebralidze, J. Poisson, F. Gaspari, E. B. Easton, O. V. Zenkina, *Mater. Adv.* **2021**, *2*, 953.
[17] S. Bin-Salamon, S. Brewer, S. Franzen, D. L. Feldheim, S. Lappi, D. A. Shultz, *J. Am. Chem. Soc.* **2005**, *127*, 5328.
[18] G. Poneti, L. Poggini, M. Mannini, B. Cortigiani, L. Sorace, E. Otero, P. Sainctavit, A. Magnani, R. Sessoli, A. Dei, *Chem. Sci.* **2015**, *6*, 2268.
[19] V. García-López, N. Giaconi, L. Poggini, J. Calbo, A. Juhin, B. Cortigiani, J. Herrero-Martín, E. Ortí, M. Mannini, M. Clemente-León, E. Coronado, *Adv. Funct. Mater.* **2023**, *n/a*, 2300351.
[20] J. Rodríguez-López, N. L. Ritzert, J. A. Mann, C. Tan, W. R. Dichtel, H. D. Abruña, *J. Am. Chem. Soc.* **2012**, *134*, 6224.
[21] F. Miomandre, E. Lépicier, S. Munteanu, O. Galangau, J. F. Audibert, R. Méallet-Renault, P. Audebert, R. B. Pansu, *Appl. Mater. Interf.* **2011**, *3*, 690.
[22] T. Ma, A. J. Grzedowski, T. Doneux, D. Bizzotto, *J. Am. Chem. Soc.* **2022**, *144*, 23428.
[23] L. Guerret-Legras, B. Maillot, J. F. Audibert, G. V. Dubacheva, L. Galmiche, P. Lang, F. Miomandre, *J. Phys. Chem. C* **2019**, *123*, 29255.
[24] B. Doppagne, M. C. Chong, H. Bulou, A. Boeglin, F. Scheurer, G. Schull, *Science* **2018**, *361*, 251.
[25] A. Loudet, K. Burgess, *Chem. Rev.* **2007**, *107*, 4891.
[26] F. Odobel, H. Zabri, *Inorg. Chem.* **2005**, *44*, 5600.
[27] A. Bakkar, F. Lafolet, D. Roldan, E. Puyoo, D. Jouvenot, G. Royal, E. Saint-Aman, S. Cobo, *Nanoscale* **2018**, *10*, 5436.
[28] A. Rosencwaig, G. K. Wertheim, H. J. Guggenheim, *Phys. Rev. Lett.* **1971**, *27*, 479.
[29] G. Beamson, D. Briggs, *High resolution XPS of organic polymers : the Scienta ESCA300 database*, Wiley, Chichester, England **1992**.
[30] C. D. Wagner, A. V. Naumkin, A. Kraut-Vass, J. W. Allison, C. J. Powell, J. R. J. Rumble, NIST Standard Reference Database 20, Version 3.4 (web version), **2003**.
[31] S. Aroua, T. K. Todorova, P. Hommes, L.-M. Chamoreau, H.-U. Reissig, V. Mougel, M. Fontecave, *Inorg. Chem.* **2017**, *56*, 5930.
[32] S. Paul, P. Kundu, P. Kondaiah, A. R. Chakravarty, *Inorg. Chem.* **2021**, *60*, 16178.
[33] J. A. Mann, J. Rodríguez-López, H. D. Abruña, W. R. Dichtel, *J. Am. Chem. Soc.* **2011**, *133*, 17614.
[34] E. Campagnoli, J. Hjelm, C. J. Milios, M. Sjodin, Z. Pikramenou, R. J. Forster, *Electrochim. Acta* **2007**, *52*, 6692.
[35] O. Mertins, O. Buriez, E. Labbé, P.-P. Fang, E. Hillard, A. Vessières, G. Jaouen, Z.-Q. Tian, C. Amatore, *J. Electroanal. Chem.* **2009**, *635*, 13.
[36] J. Chambers, B. Eaves, D. Parker, R. Claxton, P. S. Ray, S. J. Slattery, *Inorg. Chim. Acta* **2006**, *359*, 2400.
[37] K. Katayama, M. Hirotsu, A. Ito, Y. Teki, *Dalton Trans.* **2016**, *45*, 10165.
[38] Y.-Q. Li, J.-W. Dai, M. Wang, M. Yamashita, Z.-Y. Li, *Cryst. Growth Des.* **2022**, *22*, 4453.
[39] O. Galangau, I. Fabre-Francke, S. Munteanu, C. Dumas-Verdes, G. Clavier, R. Méallet-Renault, R. B. Pansu, F. Hartl, F. Miomandre, *Electrochim. Acta* **2013**, *87*, 809.
[40] D. C. Magri, *Coord. Chem. Rev.* **2021**, *426*, 213598.
[41] C. Y. Mok, A. W. Zanella, C. Creutz, N. Sutin, *Inorg. Chem.* **1984**, *23*, 2891.
[42] L. Norel, C. Tourbillon, J. Warnan, J.-F. Audibert, Y. Pellegrin, F. Miomandre, F. Odobel, S. Rigaut, *Dalton Trans.* **2018**, *47*, 8364.
[43] X. Zhang, S. Abid, L. Shi, J. A. G. Williams, M. A. Fox, F. Miomandre, C. Tourbillon, J.-F. Audibert, O. Mongin, F. Paul, C. O. Paul-Roth, *Dalton Trans.* **2019**, *48*, 11897.